HHS Public Access

Author manuscript

Neurobiol Dis. Author manuscript; available in PMC 2018 June 01.

Published in final edited form as:

Neurobiol Dis. 2017 June ; 102: 38–48. doi:10.1016/j.nbd.2017.02.006.

SCN3A deficiency associated with increased seizure susceptibility

Tyra Lamar[1,*], **Carlos G. Vanoye**[2,*], **Jeffrey Calhoun**[2,*], **Jennifer C. Wong**[1], **Stacey B.B. Dutton**[1], **Benjamin S. Jorge**[3], **Milen Velinov**[4], **Andrew Escayg**[1,†], and **Jennifer A. Kearney**[2,†]

[1]Department of Human Genetics, Emory University, Atlanta, Georgia, USA

[2]Department of Pharmacology, Northwestern University Feinberg School of Medicine, Chicago, Illinois, 60611, USA

[3]Neuroscience Program, Vanderbilt University, Nashville, Tennessee, 37232, USA

[4]New York State Institute for Basic Research in Developmental Disabilities, Staten Island, NY, USA Albert Einstein College of Medicine, Bronx, NY, USA

Abstract

Mutations in voltage-gated sodium channels expressed highly in the brain (*SCN1A*, *SCN2A*, *SCN3A*, and *SCN8A*) are responsible for an increasing number of epilepsy syndromes. In particular, mutations in the *SCN3A* gene, encoding the pore-forming $Na_v1.3$ α subunit, have been identified in patients with focal epilepsy. Biophysical characterization of epilepsy-associated *SCN3A* variants suggests that both gain- and loss-of-function *SCN3A* mutations may lead to increased seizure susceptibility. In this report, we identified a novel *SCN3A* variant (L247P) by whole exome sequencing of a child with focal epilepsy, developmental delay, and autonomic nervous system dysfunction. Voltage clamp analysis showed no detectable sodium current in a heterologous expression system expressing the SCN3A-L247P variant. Furthermore, cell surface biotinylation demonstrated a reduction in the amount of SCN3A-L247P at the cell surface, suggesting the SCN3A-L247P variant is a trafficking-deficient mutant. To further explore the possible clinical consequences of reduced *SCN3A* activity, we investigated the effect of a hypomorphic *Scn3a* allele (*Scn3a*^{Hyp}) on seizure susceptibility and behavior using a gene trap mouse line. Heterozygous *Scn3a* mutant mice (*Scn3a*$^{+/Hyp}$) did not exhibit spontaneous seizures nor were they susceptible to hyperthermia-induced seizures. However, they displayed increased susceptibility to electroconvulsive (6 Hz) and chemiconvulsive (flurothyl and kainic acid) induced seizures. *Scn3a*$^{+/Hyp}$ mice also exhibited deficits in locomotor activity and motor learning. Taken together, these results provide evidence that loss-of-function of *SCN3A* caused by reduced protein

†Corresponding Authors Andrew Escayg, Ph.D., Department of Human Genetics, Whitehead Biomedical Research Building, 615 Michael Street, Suite 301, Emory University, Atlanta, Georgia, USA 30322, Tel: 404-712-8328, aescayg@emory.edu. Jennifer A. Kearney, Ph.D., Department of Pharmacology, Searle 8-510, 320 East Superior St., Northwestern University, Chicago, IL 60611, Tel: 312-503-4894, jennifer.kearney@northwestern.edu.

*equal contribution

expression or deficient trafficking to the plasma membrane may contribute to increased seizure susceptibility.

Keywords

SCN3A; $Na_v1.3$; Focal epilepsy; Voltage-gated sodium channel; seizure susceptibility

1. Introduction

Voltage-gated sodium channels (VGSCs) are responsible for the initiation and propagation of action potentials in excitable cells such as neurons. In the mammalian brain, the most highly expressed VGSC α subunits are *SCN1A*, *SCN2A*, *SCN3A*, and *SCN8A,* which encode $Na_v1.1$, $Na_v1.2$, $Na_v1.3$, and $Na_v1.6$ respectively. Mutations in these VGSCs are responsible for an increasing number of epilepsy syndromes (Escayg et al., 2000; Estacion et al., 2014; Fung et al., 2015; Howell et al., 2015; Schwarz et al., 2016; Sugawara et al., 2001; Surovy et al., 2016). Mutations in *SCN1A* have been established as the main cause of Dravet syndrome and have also been identified in some families with generalized epilepsy with febrile seizures plus (GEFS+) (Escayg and Goldin, 2010; Scheffer et al., 2009; Volkers et al., 2011). *SCN2A* mutations have been identified in patients with benign familial neonatal-infantile seizures, and both *SCN2A* and *SCN8A* mutations have been identified in some cases of severe epileptic encephalopathies (de Kovel et al., 2014; Estacion et al., 2014; Hackenberg et al., 2014; Heron et al., 2002; Sugawara et al., 2001; Vaher et al., 2014; Veeramah et al., 2012).

To date, only a few *SCN3A* mutations have been identified in patients with focal epilepsy. Electrophysiological analysis of these mutations in either transfected rat hippocampal pyramidal neurons (Estacion et al., 2010; Holland et al., 2008) or tsA201 cells (Chen et al., 2015; Vanoye et al., 2014) revealed increased persistent sodium current or elevated ramp currents. In contrast, there is one report of an *SCN3A* mutation, N302S, identified through a genetic screen of GEFS+ patients, that resulted in depolarizing shifts in voltage-dependent activation and inactivation, as well as slower recovery from slow inactivation, thereby predicting a reduction in channel activity (Chen et al., 2015). These results suggest that both gain- and loss-of-function *SCN3A* mutations may lead to epilepsy.

Epilepsy syndromes, including those caused by sodium channel mutations, are often accompanied by neuropsychiatric comorbidities, such as anxiety, autism spectrum disorders, and intellectual disability (Baasch et al., 2014; de Kovel et al., 2014; Han et al., 2012). Consistent with this, developmental delay or behavioral abnormalities have been reported in patients with *SCN3A* mutations. For example, one patient presented with speech delay and attention-deficit/hyperactivity disorder (Vanoye et al., 2014). Another patient was diagnosed with nonverbal learning disability, and the patient carrying the N302S mutation was diagnosed with intellectual disability (Chen et al., 2014; Vanoye et al., 2014).

In this study, we report a novel *SCN3A* mutation (L247P) associated with childhood focal epilepsy and global developmental delay. Using a combination of electrophysiology and cell surface biotinylation experiments, we demonstrate that *SCN3A*-L247P encodes a trafficking

deficient channel. To more broadly investigate the possible clinical consequences of reduced *SCN3A* activity, we characterized the seizure and behavioral phenotypes of the available *Scn3a*$^{Gt(OST52130)Lex}$ mouse line, which expresses a hypomorphic *Scn3a* allele (*Scn3a*^{Hyp}). Heterozygous mutants (*Scn3a*$^{+/Hyp}$) displayed increased susceptibility to induced seizures, but did not exhibit spontaneous seizures. Additionally, *Scn3a*$^{+/Hyp}$ mice showed deficits in locomotor activity and motor learning. These observations demonstrate that reduced *SCN3A* function via reduced trafficking or expression can result in increased seizure susceptibility.

2. Material and Methods

2. 1. Clinical presentation

Parental consent for release of de-identified medical information was obtained. An 18 month-old female patient was evaluated due to concerns for global developmental delay, central hypotonia, right-sided renal pelviectasis, and microcephaly. She was the second child of a 39-year-old mother and 50-year-old father, both of whom denied consanguinity. The pregnancy was uncomplicated, amniocentesis was declined, and the child was born at full term. At birth, her weight was 2950 g (10%), her length was 50 cm (20%), and her head circumference was 33 cm (10%). Her Apgar scores were 9 and 9. At two days of age she had an episode of cyanosis, apnea, tonic posturing and bradycardia. EEG recording at that time was normal.

Beginning during the first week of life, two distinct types of episodes were observed, and occasionally coincided. The first type consists of a “scared look” followed by paroxysmal events, which include apnea, eyes rolling back, and limbs stiffening. These episodes occur approximately once a month and were subsequently identified as focal seizures. The second type of episode includes skin flushing and sweating and occurs several times a day for 30-second intervals. This clinical presentation is consistent with Harlequin syndrome, which is characterized by unilateral facial erythema with contralateral pallor that is strikingly demarcated at the midline. Although the color change is limited to the head, it can initiate on one side and shift to the other side within the same episode. This coincides with contralateral pupil dilation and ipsilateral ptosis. Video EEG at 14 months of age revealed right frontal-temporal electrographic seizures compatible with focal epilepsy. Various anticonvulsant medications were tried with limited success. The EEG abnormalities were not associated with the autonomic changes; therefore, it was concluded that the episodes of autonomic dysregulation are not epileptic by nature. The patient also developed progressive microcephaly, although her brain and cervical spine MRIs were normal. A routine cardiology examination, which included EKG, echocardiogram, and Holter monitor, showed no abnormalities. On telemetry, however, several episodes of sinus and junctional bradycardia were noted and thought to correspond with vagal activity and the Harlequin flushing. The child was also diagnosed with global developmental delay. She did not sit without support until 16 months after birth and was still unable to walk on her last evaluation at two years of age. Her speech development was also delayed. Additionally, her height, weight and head circumference were below the third percentile for two year olds. She also had trunkal hypotonia and mid-face hypoplasia.

Metabolic screening was negative. Familial Dysautonomia was ruled out by observation of normal fungiform tongue papillae and normal axon flare on intradermal histamine testing. Chromosomal microarray analysis was normal. Clinical whole-exome sequencing revealed a single, novel, *de novo* heterozygous sequence change in the gene *SCN3A*, L247P. *In silico* analysis concluded that this change was "likely pathogenic". Other changes reported were deemed as "benign" or were rare population variants inherited from an unaffected parent, suggesting they were not pathogenic (Supplemental Table 1). Results were confirmed by Sanger sequencing.

2.2. Plasmids and Cell Transfection

Electrophysiology and biochemistry experiments were conducted using tsA201 cells (HEK-293 stably transfected with SV40 large T antigen) grown at 37°C with 5% CO_2 in Dulbecco's modified Eagle's medium (DMEM) supplemented with 10% fetal bovine serum, 2 mM L-glutamine, and penicillin (50 U/ml)-streptomycin (50 μg/ml). Only cells from passage number < 13 were used. A plasmid encoding the major splice isoform of the human *SCN3A* with exon 5 adult (5A) and exon 12v1 (646 bp) splice variants was used (Wang et al., 2010). Full-length $Na_v1.3$ was propagated in STBL2 cells at 30°C (Invitrogen), and the open reading frame of all plasmid preparations was fully sequenced prior to transfection. The L247P variant was introduced by site-directed mutagenesis. Plasmids encoding the human Na_v channel accessory subunits β1 or β2 in vectors containing the marker genes CD8 (pCD8-IRES-β1) or GFP (pGFP-IRES-β2) were also used.

For electrophysiology experiments, expression of $Na_v1.3$, β1, and β2 subunits was achieved by transient transfection (2 μg of total cDNA: *SCN3A*, β1, β2 mass ratio was 10:1:1) using Superfect Transfection Reagent (QIAGEN, Valencia, CA, USA). Cells were incubated as described above for 48 hours after transfection before use in electrophysiology experiments. For low temperature rescue experiments, cells were incubated for 24 hours at 37°C followed by 24 hours at 28°C prior to electrophysiology. Transfected cells were dissociated by brief exposure to trypsin/EDTA, resuspended in supplemented DMEM medium, plated on glass coverslips, and allowed to recover for ~2 hrs at 37°C or 28°C in 5% CO_2. Polystyrene microbeads pre-coated with anti-CD8 antibody (Dynabeads M-450 CD 8, Dynal, Great Neck, NY, USA) were added and only cells positive for both CD8 antigen (i.e., β1 expression) and GFP fluorescence (i.e., β2 expression) were studied.

For cell surface biotinylation experiments, expression of $Na_v1.3$, β1 and β2 subunits was achieved by transient transfection (2 μg of total cDNA: *SCN3A*, β1, β2 mass ratio was 10:1:1) using Lipofectamine 2000 (Life Technologies, Grand Island, NY, USA). Before use in these experiments, cells were incubated as described above for 48 hours after transfection.

2.3. Electrophysiology

Coverslips were placed into a recording chamber on the stage of an inverted epifluorescence microscope (IX 50, Olympus, Center Valley, PA, USA) and allowed to equilibrate for 10 min in bath solution prior to starting experiments. Bath solution contained (in mM): 145 NaCl, 4 KCl, 1.8 $CaCl_2$, 1 $MgCl_2$, 10 HEPES (N-(2-hydroxyethyl) piperazine-N′-2-ethanosulphonic acid), pH 7.35, 310 mOsm/kg. The composition of the pipette solution was (in mM): 10

NaF, 110 CsF, 20 CsCl, 2 EGTA (ethyleneglycol-bis-(β-aminoethylether), 10 HEPES, pH 7.35, 310 mOsm/kg. Osmolarity and pH values were adjusted with sucrose and NaOH, respectively. A 2% agar-bridge with composition similar to the bath solution was utilized as a reference electrode. Junction potentials were zeroed with the filled pipette in the bath solution. Unless otherwise stated, chemicals were obtained from Sigma-Aldrich (St. Louis, MO, USA).

Patch pipettes were pulled from thin-wall borosilicate glass (World Precision Instruments, Inc., Sarasota, FL, USA) using a multistage P-97 Flaming-Brown micropipette puller (Sutter Instruments Co., San Rafael, CA, USA) and fire-polished with a Micro Forge MF 830 (Narashige, Japan). After heat polishing, the resistance of the patch pipettes was 1–3 MΩ in standard bath and pipette solutions. Once whole-cell recording mode was achieved, the access resistance averaged 2.5 ± 0.1 MΩ. Whole-cell sodium currents were recorded as previously described (Lossin et al., 2002; Vanoye et al., 2006) at room temperature (20–23°C) in the whole-cell configuration of the patch-clamp technique (Hamill et al., 1981) using an Axopatch 200B series amplifier (Molecular Devices Corp, Sunnyvale, CA, USA). Cells were allowed to equilibrate for 10 min after establishment of the whole-cell configuration before currents were recorded. Pulse generation was performed with Clampex 8.1 (Molecular Devices Corp.) and whole-cell currents were acquired at 20 kHz and filtered at 5 kHz. Linear leak and residual capacitance artifacts were subtracted out using the P/4 method. To reduce voltage errors, 80–90% series resistance and prediction compensation were applied. Cells were excluded from analysis if the predicted voltage error exceeded 3 mV or the current at the holding potential (−120 mV) was >5% of the peak current.

Peak currents were measured using 20 ms pulses between −80 and +50 mV every 5 s from a holding potential of −120 mV. The peak current was normalized for cell capacitance and plotted against voltage to generate peak current density–voltage relationships.

Data were collected from at least 2 transient transfections per experimental condition. Results are reported as means ± SEM, and number of cells used for each experimental condition are listed on the legends or figures. Current values were normalized to membrane capacitance.

2.4. Cell Surface Biotinylation

Forty-eight hours post-transfection, cell surface proteins of transfected tsA201 cells were labeled with cell membrane impermeable Sulfo-NHS-Biotin (Thermo Scientific, Waltham, MA, USA). The biotinylation reaction was quenched with 100mM glycine, and the cells were subsequently lysed with RIPA lysis buffer (Thermo Scientific) containing Complete protease inhibitors (Roche Applied Science, Indianapolis, IN, USA) and clarified by centrifugation. An aliquot of the supernatant was retained as the total protein fraction. Biotinylated surface proteins (300 to 600 μg per sample) were recovered from the remaining supernatant by incubation with streptavidin-agarose beads (Thermo Scientific) and elution in Laemmli sample buffer. Total (5 to 10 μg per lane) and surface fractions were analyzed by Western blotting using rabbit anti-pan VGSC α subunit (1:250; Alomone, Jerusalem, Israel), mouse anti-transferrin receptor (1:500; Life Technologies), and rabbit anti-calnexin (H70) (1:250; Santa Cruz Biotechnology, Dallas, TX, USA) primary antibodies. Peroxidase-

conjugated mouse anti-rabbit immunoglobulin G (IgG; 1:20,000; Jackson ImmunoResearch, West Grove, PA, USA) and goat anti-mouse IgG (1:40,000, Jackson ImmunoResearch) secondary antibodies were utilized. Blots were probed for each protein in succession, stripping in between with Restore Western Blot Stripping Buffer (Pierce Biotechnology, Rockford, IL, USA). Calnexin immunoreactivity was present in total protein lysates and absent from cell surface fraction, confirming the selectivity of biotin labeling for cell surface proteins. Densitometry was performed using NIH ImageJ software. Transferrin receptor was utilized as a loading control for $Na_v1.3$ immunoreactive bands. Surface fractions were analyzed from two independent transfections, while total fractions were analyzed from three independent transfections.

2.5. Mouse Model

The *Scn3a*$^{Gt(OST52130)Lex}$ mouse line (Lexicon Pharmaceuticals Inc.), containing a gene trap vector upstream of the first coding exon, was purchased from the Mutant Mouse Regional Resource Center (University of North Carolina at Chapel Hill, NC, USA). The line was maintained by backcrossing to C57BL/6J mice (Jackson Laboratories, Bar Harbor, ME, US). RNA and protein analysis in adult mice as well as all seizure and behavioral experiments were performed on heterozygous mutants and WT littermates generated by crossing N6-N7 *Scn3a*$^{+/Hyp}$ males to C57BL/6J females. WT, heterozygous, and homozygous littermates (P1) that were used for RNA and protein analysis were generated by mating heterozygous siblings from the N8-N9 generations. Mice were housed in an animal facility with a 12-hour light/dark cycle (lights on 7:00am – lights off 7:00pm) with food and water available *ad libitum*. All experiments were performed in accordance with the guidelines of the Emory University Institutional Animal Care and Use Committees. Unless stated otherwise, adult (4–6 month old) mice were used for the following experiments.

2.6. Genotyping

Genotyping was performed on DNA extracted from tail biopsies. To detect the wild-type allele, forward and reverse PCR primers were designed in the intronic sequences flanking the vector insertion site (3AF: GAGGATCAGGCTTAGCGGTG; 3AR: TCTGGTCTGTTATGTCAGAAGGC) to produce a 337 bp PCR product. To detect the mutant allele, a forward primer was designed in the vector sequence (VECTF: TATGTATTTTTCCATGCCTTGC) and paired with the 3AR reverse primer to produce a 233 bp PCR product.

2.7. Quantitative real-time PCR (qRT-PCR)

Total RNA was extracted from whole brain samples of 1-day old (P1) homozygous (*Scn3a*$^{Hyp/Hyp}$; n = 3) and heterozygous (*Scn3a*$^{+/Hyp}$; n = 5) mutants and wild-type (WT; n = 4) littermates. RNA extraction and cDNA synthesis were performed as previously described (Makinson et al., 2014). PCR amplification of *Scn1a*, *Scn2a*, *Scn3a* and *Scn8a* was performed using primers designed to span two exons. The following primer pairs were used: *Scn1a* (F: CAGGAGGAAGGGGTTTCGCTTC, R: CCCCACATCCTTGGCTCGCCCTC), *Scn2a* (F: CTGCAACGGTGTGGTCTCCCTAG, R: ATGTAGGGTCTTCCAACAAGTCC), *Scn3a* (F: CCTGGACCCCTACTACGTCA, R: TGTGTACTCTACATTCTTCGTCCA), and *Scn8a* (F: AGATTTAGCGCCACTCCTGC, R: GGACCATTCGGGAGGGTTAC). Each

primer pair produced standard curves with 90–100% efficiency. Real-time analysis was performed in technical triplicate using the BioRad CFX96 Real-Time PCR Detection System and SYBR Green fluorescent dye (BioRad, Hercules, CA, USA). Expression levels were normalized to beta-actin (F: CAGCTTCTTTGCAGCTCCTT, R: ACGATGGAGGGGAATACAGC). Expression relative to WT was determined using the Pfaffl calculation (Pfaffl, 2001).

2.8. Western Blot Analysis

Whole brains were extracted from P1 WT (n = 5), *Scn3a*$^{+/Hyp}$ (n = 6), and *Scn3a*$^{Hyp/Hyp}$ littermates (n = 4). Tissue was homogenized with a Dounce homogenizer in cold protease inhibitor buffer (50mM Tris, pH 7.5; 10mM EGTA; 1 protease inhibitor cocktail tablet (Roche) per 50mL of buffer). The homogenate solution was centrifuged at 3500 RPM for 10 minutes at 4°C. The resulting supernatant was centrifuged at 38,000 RPM for 30 minutes at 4°C. The membrane-enriched pellet was resuspended in protease inhibitor buffer and then stored at −80°C. Protein was quantified using the BCA protein assay (Pierce, Rockford, Il, USA). The protein (50 μg) was then denatured, separated by SDS-PAGE, and transferred to PVDF membrane. The membranes were blocked with 5% milk, then incubated at 4°C overnight with either polyclonal rabbit anti-$Na_v1.1$ (1:200; Millipore, Billerica, MA), $Na_v1.2$ (1:200; Millipore), Nav1.3 (1:200; Alomone), or $Na_v1.6$ (1:200; Millipore), followed by HRP-conjugated donkey anti-rabbit secondary antibody (1:3000; GE Healthcare Life Sciences, Little Chalfont, UK) for 1 hour. To normalize for variation in protein loading, membrane blots were also incubated for 1 hour with monoclonal mouse anti-tubulin (1:5000; Sigma-Aldrich) followed by HRP-conjugated goat anti-mouse secondary antibody (1:3000; Jackson ImmunoResearch). Following each secondary antibody, all blots were incubated in HyGlo Quick Spray (Denville Scientific, Holliston, MA, USA) and imaged. Protein expression was quantified using Image J software (NIH).

2.9. Hyperthermia-induced Seizures

Susceptibility to hyperthermia-induced seizures in P21–22 *Scn3a*$^{+/Hyp}$ mutants (n = 12) and WT littermates (n = 13) was determined as previously described (Dutton et al., 2013). Since mice are not sexually mature at this age, results from male and female mice were combined. Briefly, the body temperature of each mouse was monitored and controlled via a rectal temperature probe that was connected to a heating lamp and temperature controller (TCAT 2DF, Physitemp, Clifton, NJ, USA). Each mouse was placed in a clear cylinder and held at 37.5°C for 10 minutes. The core body temperature of each mouse was then increased by 0.5°C every two minutes until either a seizure occurred or a temperature of 42.5°C was reached. The temperature at which each mouse exhibited a GTCS was compared between genotypes. Behavioral seizures were also scored using a modified Racine scale (Racine, 1972): 1 – staring, 2 – head nodding, 3 – unilateral forelimb clonus, 4 – bilateral forelimb clonus, 5 – rearing and falling, 6 – generalized tonic-clonic seizure (GTCS).

2.10. 6 Hz Seizure Induction

The topical anesthetic tetracaine (0.5%, Bausch and Lomb, Rochester, NY, USA) was applied to each eye 30 minutes prior to seizure induction. Adult male *Scn3a*$^{+/Hyp}$ mutants and WT littermates (n = 10/genotype) were subjected to 6 Hz corneal stimulation (0.2 ms

pulse width, 3 s duration) using an ECT unit (Ugo Basile; Comerio, Italy). Each mouse was tested once per week, over a 3-week period, using a current of 16, 24, or 30 mA. Behavioral seizures were scored using a modified Racine scale: 0 – no seizure, 1 – staring, 2 – forelimb clonus, and 3 – rearing and falling. For each genotype, the CC_{50} (the convulsive current at which 50% of mice seize) was established as well as the average Racine scores at each current.

2.11. Flurothyl Seizure Induction

Seizure induction using flurothyl (2,2,2-trifluroethyl ether, Sigma-Aldrich) was performed as previously described (Makinson et al., 2014; Martin et al., 2007; Sawyer et al., 2014). Briefly, 5–8 week old *Scn3a*$^{+/Hyp}$ male and female mutants (n = 29/sex) and WT littermates (male n = 33; female n = 32) were placed in a clear chamber and flurothyl was introduced at a constant rate of 20 μl/min. Latencies to the first myoclonic jerk, first generalized tonic-clonic seizure (GTCS) with loss of posture, and hind limb extension were recorded.

2.12. EEG cortical/depth electrode surgery

Electroencephalogram (EEG) electrodes were surgically implanted in adult male *Scn3a*$^{+/Hyp}$ mice (n = 6) and WT littermates (n = 4) as previously described (Dutton et al., 2013; Makinson et al., 2014; Martin et al., 2007; Papale et al., 2013). Briefly, two pairs of bipolar stainless steel screw electrodes (Vintage Machine Supplies, OH, USA) were implanted in the skull at the following coordinates (relative to bregma): anterior-poster (AP) +0.5 mm and medial-lateral (ML) −2.2 mm; AP +2.0 mm and ML +1.2 mm; AP −3.5 mm and ML −2.2 mm; AP −1.5 mm and ML +1.2 mm. Two fine-wire electrodes were implanted in the dorsal neck muscles to record electromyography (EMG) activity.

Depth EEG recordings were obtained in adult male *Scn3a*$^{+/Hyp}$ mice (n = 3) and WT littermates (n = 2). Two depth electrodes were implanted into the hippocampus (relative to bregma): AP −1.8 mm, ML ±1.6 mm, dorsal-ventral (DV) −1.7 mm. Two cortical electrodes were also implanted (relative to bregma): AP +2.0 mm and ML+1.2 mm; AP +0.5 mm and ML −2.2 mm. EMG electrodes were not implanted for depth EEG recordings.

For all surgeries, mice were administered Meloxicam (2 mg/kg; Norbrook Laboratories, Lenexa, KS, USA) preoperatively and postoperatively for two days following surgery (1 mg/kg). Each mouse was allowed to recover from surgery for at least 7 days before the onset of EEG recording. Twelve days of continuous video/EEG recording were collected from each mouse, and EEG signals were analyzed with Stellate Harmonie EEG software (Natus Medical Inc., San Carlos, CA, USA) using a high-pass filter of 0.5 Hz and a low-pass filter of 35 Hz. For the cortical-only recordings, EMG signals were analyzed using a high-pass filter of 10 Hz and a low-pass filter of 70 Hz. Two montages were used to manually score the cortical-only and depth EEG recordings. In the first montage, one muscle electrode was used as the reference. Since muscle electrodes were not implanted during the depth electrode surgery, the second montage used a cortical electrode as a reference. Seizure activity was defined as synchronous discharges of increasing frequency with amplitudes at least twice the background.

2.13. Kainic Acid Seizure Induction

Male *Scn3a*$^{+/Hyp}$ mutants (n = 8) and WT littermates (n = 5) were administered kainic acid (i.p., 20 mg/kg, Sigma-Aldrich) and observed for two hours. Seizures were confirmed by EEG analysis using cortical electrode and hippocampal depth electrodes as described above. Behavioral seizures were scored using a modified Racine scale: 0 – no behavior, 1 – freezing/staring, 2- head nodding, 3 – tail clonus, 4 – forelimb clonus, 5 – rearing and falling, and 6 – death (Makinson et al., 2014; Martin et al., 2007; Tang et al., 2009). The latency to the first electrographic seizure in each mouse as well as the average seizure severity during the observation period were compared.

2.14. Locomotor Activity

Adult male *Scn3a*$^{+/Hyp}$ mice and WT littermates (n= 8/genotype) were placed in novel transparent cages (40 × 20 × 20 cm) equipped with 7 infrared photobeams, each beam spaced 5 cm apart and 5 cm from the cage wall (San Diego Instruments Inc., San Diego, CA, USA). Activity was monitored for 48 hours, and ambulation was recorded as the number of consecutive beam breaks during the time period.

2.15. Rotarod

Adult male *Scn3a*$^{+/Hyp}$ mice (n =11) and WT littermates (n= 9) were trained on a fixed speed (5 RPM) rotating rod (AccuScan Instruments, Columbus, OH, USA) daily for five minutes across two days. Experimental trials were performed on an accelerating (acceleration: 4–40 RPM) rotarod (Columbus Instruments, Columbus, OH, USA) for three days following training. Animals were subjected to three 5-minute trials each day, with a rest period of 30 minutes between each trial. The latency to fall was recorded for each trial.

2.16. Statistical Analysis

Data was analyzed using the following software: Clampfit 8.1 (Molecular Devices Corp.), Excel 2002 (Microsoft, Seattle, WA, USA), SigmaPlot 10 (Systat Software, Inc., San Jose, CA, USA), Prism 5–6 (GraphPad Software, Inc., La Jolla, CA, USA), and SPSS Statistical Software (IBM, Armonk, NY, USA). mRNA expression (normalized to β-actin), protein expression (normalized to α-tubulin and reported in optical density units), latencies to flurothyl-induced seizures, and latencies to the first KA-induced electrographic seizure were analyzed with a two-tailed Student's t-test when comparing two genotypes or one-way Analysis of Variance (ANOVA) followed by the Tukey pairwise *post hoc* comparison when comparing three genotypes. The log-rank (Mantel-Cox) test was used to analyze the number of animals that seized in the hyperthermia-induced seizure paradigm and the temperature at which each mouse seized per genotype. The 6 Hz CC_{50} and respective confidence intervals were determined for each genotype using log-probit analysis. Racine scores at each current in the 6 Hz paradigm were analyzed using the nonparametric Mann-Whitney Rank Sum test. A two-way repeated measures ANOVA followed by Bonferroni's multiple comparisons *post hoc* analyses was used to analyze the time course of KA-induced seizure severity, the number of ambulations during locomotor activity, and latency to fall during the rotarod task. All bar graphs indicate the means, and all error bars represent ± standard error of the mean (SEM).

3. Results

3.1. The SCN3A-L247P variant is associated with childhood epilepsy and encodes a trafficking deficient channel

Clinical whole-exome sequencing identified a single de novo variant, SCN3A-L247P, in an 18 month-old female patient exhibiting focal seizures, global developmental delay, and autonomic dysfunction. This non-synonymous variant was not present in either parent, or in publically available exome databases (Exome Aggregation Consortium (ExAC), 2016; Exome Variant Server, 2016). *SCN3A* is highly intolerant of variation with genic intolerance score of −2.48 for missense variants, putting it amongst the top 1% most intolerant of genes (Petrovski et al., 2013). The SCN3A-L247P variant resulted in a non-conservative amino acid substitution at the cytoplasmic face of the S5 transmembrane segment in domain 1 (Fig. 1A and 1B). We attempted to functionally characterize this variant using recombinant human $Na_v1.3$ co-expressed with human β1 and β2 subunits in a heterologous expression system (tsA201 cells). However, SCN3A-L247P mutant channels failed to exhibit significant sodium current (Fig. 1C–D). Incubation at low temperature (28°C) for 24 hours did not rescue any significant sodium current (Fig. 1D). Two independent recombinant $Na_v1.3$ clones expressing the L247P mutation were tested. The open reading frame of both clones was fully sequenced to rule out cloning artifacts.

The absence of detectable sodium current in cells transfected with SCN3A-L247P suggests that either the mutation affected the level of channel protein at the cell surface, or the mutant channel is expressed at the cell surface but does not conduct sodium. To determine the level of cell surface expression of SCN3A-L247P, we performed cell surface biotinylation (Fig. 1E). There was a significant reduction in the amount of SCN3A-L247P at the level of the cell surface relative to SCN3A-WT (normalized surface VGSC expression = 1.0 for SCN3A-WT and 0.18 for SCN3A-L247P; n = 2). There was also a trend toward a decrease in total cellular SCN3A expression between SCN3A-WT and SCN3A-L247P (normalized total VGSC expression = 1.0 for SCN3A-WT and 0.66 for SCN3A-L247P; p = 0.11, Student's t-test; n = 3). Fewer $Na_v1.3$ channels at the cell surface would be predicted to reduce the magnitude of the inward current, which may contribute to disease pathogenesis.

3.2. Scn3a mRNA and protein expression is reduced in $Scn3a^{+/Hyp}$ and $Scn3a^{Hyp/Hyp}$ mice

To better understand the contribution of *SCN3A* to disease, we evaluated the *Scn3a* gene trap mouse line, $Scn3a^{Gt(OST52130)Lex}$, developed by Lexicon Pharmaceuticals. The original description of this mouse line reported the observation of only two homozygotes from 63 pups at the F2 generation (WT: 20, heterozygous: 41, homozygous: 2; Chi-squared: 16.016, df = 2, $p < 0.001$), neither of which survived beyond four weeks of age (http://www.informatics.jax.org/external/ko/lexicon/1392.html; Lexicon personal communication). We generated WT, heterozygous, and homozygous pups for our study by mating heterozygous siblings that had been backcrossed 8–9 generations onto the C57BL/6J strain. Although fewer homozygotes were born than WT pups, we did not observe statistically significant deviations from Mendelian ratios in animals born (WT: 21, heterozygous: 36, homozygous: 10; Chi-squared: 3.985, df = 2, p = 0.14). However, in order to appropriately model the heterozygous *SCN3A* mutation observed in the patient, we used heterozygous

mutants and WT littermates, generated from crossing male heterozygous mutants to female C57BL/6J mice, for all behavioral experiments. Gross brain morphology of adult heterozygous mutants was normal except for focal cortical anomalies, including disruptions in cortical lamination and invaginations (Supplemental figure 1). These were observed in the majority of *Scn3a*$^{+/Hyp}$ mice examined, but not in WT littermates. However, cortical malformations have been reported to occur in WT C57BL/6J mice at a low level (Ramos et al., 2008). To confirm disruption of *Scn3a* in mutant mice, quantitative real-time PCR analysis was performed on whole brain samples from one-day old (P1) WT, heterozygous and homozygous littermates. We observed approximately 70% and nearly 100% reduction of *Scn3a* mRNA expression (relative to WT) in the brains of heterozygous and homozygous mutants, respectively ($p < 0.0001$, Fig. 2A). Western blotting indicated that $Na_v1.3$ protein expression in the brains of P1 heterozygous and homozygous mutants, compared to WT, was reduced by approximately 35% ($p < 0.05$) and 60% ($p < 0.001$), respectively (Fig. 2B). These observations indicate that the *Scn3a* gene trap allele is hypomorphic (defined henceforth as *Scn3a*^{Hyp}). In adult heterozygous *Scn3a*$^{+/Hyp}$ mice, *Scn3a* mRNA expression was reduced by approximately 60% compared to WT in both the hippocampus and cerebellum ($p < 0.05$; Supplemental Fig. 2A). $Na_v1.3$ protein expression was undetectable in the brains of adult WT and *Scn3a*$^{+/Hyp}$ mice.

To determine whether *Scn3a* deficiency could alter the expression levels of other CNS VGSCs, we compared *Scn1a*, *Scn2a*, and *Scn8a* mRNA and protein levels from the brains of *Scn3a*^{Hyp} mutant mice and WT littermates. Although *Scn1a* (Fig. 3A), *Scn2a* (Fig. 3B), and *Scn8a* (Fig. 3C) mRNA levels were comparable between P1 *Scn3a*$^{+/Hyp}$ pups and WT littermates, they were significantly reduced in *Scn3a*$^{Hyp/Hyp}$ pups ($p < 0.05$). No significant differences in mRNA expression of *Scn1a*, *Scn2a*, and *Scn8a* were observed between adult *Scn3a*$^{+/Hyp}$ mice and WT littermates (Supplemental Fig. 2B–D). $Na_v1.1$, $Na_v1.2$, and $Na_v1.6$ protein expression was undetectable by Western blotting for all genotypes of P1 mice (data not shown). No significant differences in protein levels of $Na_v1.1$, Na_v 1.2 and Na_v 1.6 were observed in adult *Scn3a*$^{+/Hyp}$ mutant mice compared with WT littermates (Supplemental Fig. 2B–D).

3.3. Scn3a$^{+/Hyp}$ mice exhibit increased seizure susceptibility

We first determined whether reduced *Scn3a* expression increases susceptibility to hyperthermia-induced seizures. Core body temperature of P21-P22 *Scn3a*$^{+/Hyp}$ mutants and WT littermates was increased by 0.5°C every two minutes until either a generalized tonic-clonic seizure (GTCS) was observed or 42.5°C is reached. No statistically significant differences were observed in the number of mice exhibiting seizures, the temperature at which the seizure occurred, nor the seizure severity between *Scn3a*$^{+/Hyp}$ mice and WT littermates (Fig. 4).

Next, we assessed the susceptibility of male *Scn3a*$^{+/Hyp}$ mutants to focal seizures using the 6 Hz “psychomotor” seizure induction paradigm (Brown et al., 1953; Toman, 1951). Male *Scn3a*$^{+/Hyp}$ mutants and WT littermates were tested at current intensities of 16 mA, 24 mA, and 30 mA. Seizure incidence and severity (based on a modified Racine score, denoted RS) was compared between *Scn3a*$^{+/Hyp}$ mutants and WT littermates at each current (Fig. 5).

Both genotypes displayed minimal seizure response at 16 mA. However, at 24 mA, 50% (5/10) of *Scn3a*$^{+/Hyp}$ mutants seized (3RS1, 2RS2), compared with 10% (1/10) of WT (1RS3). At 30 mA, 90% (9/10) *Scn3a*$^{+/Hyp}$ mutants seized (4RS1, 3RS2, 2RS3) compared with 56% (5/9) of WT littermates (1RS1, 1RS2, 3RS3). Based on these results, the CC_{50} was found to be significantly lower in the *Scn3a*$^{+/Hyp}$ mutants [CC_{50} = 24 mA; 95% CI: 19.8 to 25.4] when compared with WT littermates [CC50 = 29 mA; 95% CI: 26.7 to 38.4] (Fig. 5A). No statistically significant differences were observed in seizure severity between mutant and WT littermates at the currents tested (Fig. 5B).

Latencies to flurothyl-induced seizures were examined in both sexes of *Scn3a*$^{+/Hyp}$ mutants and WT littermates (Fig. 6). The average latency to the first myoclonic jerk was reduced in *Scn3a*$^{+/Hyp}$ mutants compared to WT littermates in both sexes. Average latencies to the first GTCS were comparable between male *Scn3a*$^{+/Hyp}$ mutant and male WT littermates (Fig. 6A); however, female *Scn3a*$^{+/Hyp}$ mutants exhibited significantly reduced latencies to the GTCS when compared to female WT littermates ($p < 0.01$, Fig. 6B). In both sexes, *Scn3a*$^{+/Hyp}$ mice progressed to hindlimb extension significantly faster than WT littermates (male: $p < 0.001$; female: $p < 0.001$).

The response of male *Scn3a*$^{+/Hyp}$ mutants and WT littermates to kainic acid (KA)-induced seizures was also compared (Fig. 7). *Scn3a*$^{+/Hyp}$ mutants exhibited significantly higher average Racine scores compared to WT littermates from 20 minutes to 2 hours following KA administration ($p < 0.05$, Fig. 7A). The latency to the first observed electrographic seizure was also significantly reduced in *Scn3a*$^{+/Hyp}$ mice ($p < 0.05$, Fig. 7B). An example of an EEG-confirmed KA-induced seizure in a *Scn3a*$^{+/Hyp}$ mutant is shown in Fig. 7C.

3.4. Scn3a$^{+/Hyp}$ mutants do not exhibit spontaneous seizures

Male *Scn3a*$^{+/Hyp}$ mutants (n= 6) and WT littermates (n= 4) were implanted with cortical electrodes and continuous video/EEG analysis was performed for 12 days (288 hours each mouse). No spontaneous seizures were detected during the recording period. Since patients with *SCN3A* mutations exhibit focal seizures, we also performed EEG analysis on *Scn3a*$^{+/Hyp}$ mice (n= 3) and WT littermates (n = 2) using depth electrodes positioned bilaterally in the dorsal hippocampus. Each mouse was continuously monitored by video/EEG analysis for 12 days; however, no spontaneous seizures were detected.

3.5. Scn3a$^{+/Hyp}$ mutants are hypoactive and display deficits in motor learning

The locomotor activity of male *Scn3a*$^{+/Hyp}$ mice and WT littermates was continuously monitored for 48 hours and the number of ambulations were recorded (Fig. 8A). *Scn3a*$^{+/Hyp}$ mutants traveled significantly less than WT littermates during the first dark cycle (8:00–11:00 pm; hours 6.5 to 9.5) and during the second dark cycle (9:00 – 9:30 pm; hours 31.5–32.0) ($p < 0.05$, Fig. 8A). We also compared motor learning between *Scn3a*$^{+/Hyp}$ mice and WT littermates using an accelerating rotarod. All mice underwent three trials per day for three days. There were no differences in average latencies to fall between the genotypes during the first five trials. During the remaining trials, however, *Scn3a*$^{+/Hyp}$ mutants fell from the accelerating rotarod significantly faster than WT littermates (Fig. 8B). A battery of behavioral tests was also conducted on the *Scn3a*$^{+/Hyp}$ mutants and WT littermates to

evaluate exploratory activity, anxiety, memory, social behavior, depressive-like behavior, vision, and sensorimotor gating (Supplemental Table 2). No statistically significant differences were observed between mutants and WT littermates in any of these behavioral tasks, with the exception of the open field in which *Scn3a*$^{+/Hyp}$ mice entered the center zone significantly fewer times when compared to WT littermates ($p < 0.05$).

4. Discussion

4.1. A novel SCN3A variant (L247P) is associated with childhood epilepsy and displays reduced trafficking to the cell surface

Clinical whole-exome sequencing identified a novel, non-synonymous missense variant in the *SCN3A* gene, encoding the $Na_v1.3$ VGSC α subunit, in a female patient with childhood epilepsy, global developmental delay, and autonomic nervous system dysfunction. The L247P substitution replaces a highly conserved leucine residue with proline at the cytoplasmic face of the DIS5 transmembrane domain (Fig. 1B). This substitution is predicted to affect the secondary structure of *SCN3A*, which could alter the function or trafficking of the channel (Supplemental Table 1). We demonstrate herein that SCN3A-L247P is a trafficking deficient mutant. This finding provides further support for loss-of-function of *SCN3A* as a pathogenic mechanism.

There is a precedent for the rescue of trafficking-deficient sodium channel mutants by co-expression of VGSC β subunits, other interacting proteins, or pharmacologic agents (Bechi et al., 2015; Cestele et al., 2013; Rusconi et al., 2009; Rusconi et al., 2007; Thompson et al., 2012). The biochemical and functional assays of SCN3A-L247P were performed in cells co-transfected with β1 and β2 subunits, suggesting that β1 and β2 are not sufficient to rescue the trafficking of SCN3A-L247P. Further experimentation will be necessary to ascertain whether the trafficking of SCN3A-L247P can be rescued by other interacting proteins or pharmacologic agents.

4.2. In vivo characterization of Scn3a haploinsufficiency

In order to further explore the potential of reduced *SCN3A* activity to confer elevated seizure risk *in vivo*, we studied the gene trapped *Scn3a*$^{Gt(OST52130)Lex}$ line. *Scn3a* mRNA expression in P1 mice was found to be significantly reduced in heterozygous mutants, and $Na_v1.3$ protein levels were approximately 35% lower than in WT littermates. Interestingly, although *Scn3a* mRNA in homozygous mutants was almost undetectable, $Na_v1.3$ protein was still detected, indicating that this mouse line is hypomorphic. It is well recognized that mRNA and protein expression levels do not always correlate due to experimental noise, the stability of the RNA or protein, or modifications at the transcriptional or translational level (Maier et al., 2009; Nie et al., 2006; Raj et al., 2006). We were unable to detect $Na_v1.3$ protein in the adult WT mouse brain by Western blot, which is consistent with observations from a previous study (Cheah et al., 2013). The lack of detectable $Na_v1.3$ protein in adult brain also confirmed the specificity of the Scn3a antibody, since we showed that all other CNS VGSCs are detectable in the adult brain.

Previous observations by Lexicon indicated reduced viability of homozygous *Scn3a*$^{Hyp/Hyp}$ mutants, suggesting that *Scn3a* is critical during early development. In the current study, we did not observe significant skewing of Mendelian ratios when the three genotypes (WT, *Scn3a*$^{+/Hyp}$, *Scn3a*$^{Hyp/Hyp}$) were examined at P1. However, Lexicon observations were based on numbers at the time of genotyping (P10 at earliest); therefore, homozygous mutants likely exhibit postnatal lethality. We also investigated whether the expression of the other brain VGSCs would be altered due to the reduced expression of *Scn3a*. Previous studies have demonstrated that sodium channel deficiency can result in changes in expression of other VGSCs. For example, *Scn1b*-null mice exhibit reduced $Na_v1.1$ and increased $Na_v1.3$ protein levels (Chen et al., 2004). Analysis of *Scn1a* knockout mice also showed compensatory upregulation of $Na_v1.3$ in hippocampal interneurons, although this increase was insufficient to restore normal levels of sodium current (Yu et al., 2006). In the current study, *Scn1a*, *Scn2a*, and *Scn8a* mRNA levels were unchanged in P1 *Scn3a*$^{+/Hyp}$ mice, while mRNA expression was significantly reduced in homozygous mutants. However, since $Na_v1.1$, $Na_v1.2$, and $Na_v1.6$ proteins are undetectable by Western blot in P1 mice, further investigation will be required to determine whether these observed reductions in mRNA levels are functionally important.

To date, only two reported patients with *SCN3A* mutations (M1323V, N302S) have presented with febrile seizures, suggesting that this is not a common seizure type for *SCN3A* mutations (Chen et al., 2015; Vanoye et al., 2014). Consistent with clinical observations, *Scn3a*$^{+/Hyp}$ mice did not show increased susceptibility to hyperthermia-induced seizures. However, *Scn3a*$^{+/Hyp}$ mice did exhibit increased susceptibility to flurothyl, KA, and 6 Hz-induced seizures. The results from the KA and the 6 Hz paradigms are particularly relevant since these approaches model limbic seizures, which are the most commonly observed seizure type in patients with *SCN3A* mutations, including the patient with the L247P mutation (Barton et al., 2001; Holland et al., 2008; Vanoye et al., 2014). Taken together, these clinical and experimental findings suggest a role for *SCN3A* in the development of generalized and partial epilepsy.

While the *Scn3a*$^{+/Hyp}$ mutant did not express the L247P mutation identified in the patient, the observation of increased seizure susceptibility in the mutants provides support for the association between reduced *SCN3A* activity and increased seizure susceptibility. Although we did not observe spontaneous seizures in the *Scn3a* mice, we cannot exclude the possibility of infrequent seizures that were not captured during the periods of EEG analysis. It is noteworthy that two of the six *Scn3a*$^{+/Hyp}$ mice fitted with cortical electrodes were observed exhibiting brief, seizure-like behaviors, including rearing and falling. However, these behaviors did not correspond with electrographic seizure activity. Furthermore, we cannot exclude the possibility that the spontaneous seizures in the patient are the result of the toxic accumulation of mutant $Na_v1.3$ protein in the cells due to defective trafficking.

One general caveat of mouse models is that gene expression patterns can differ from humans. *SCN3A* is highly expressed during early development in humans and rodents, with expression declining into adulthood (Black et al., 1994; Chen et al., 2000; Felts et al., 1997; Whitaker et al., 2001). However, the relative reduction in adult *Scn3a* levels appears to be greater in the mouse. Nevertheless, a number of studies have revealed that *Scn3a* expression

is still detectable in certain brain regions, including the hippocampus and cortex, during adulthood (Beckh et al., 1989; Furuyama et al., 1993; Lindia and Abbadie, 2003). The observation of increased seizure susceptibility in *Scn3a*$^{+/Hyp}$ mutants suggest that *Scn3a* is still functionally important in the adult mouse. However, it is also possible that reduced *Scn3a* during early development results in long-term alterations in neuronal excitability or cortical organization. Future studies will investigate these possibilities.

4.3. A putative role for Scn3a in motor function and coordination

Scn3a$^{+/Hyp}$ mice exhibited reduced locomotor activity, suggesting hypoactivity, and decreased latency to fall from a rotarod. Interestingly, average latencies to fall from the rotarod were not significantly different between the genotypes during the initial trials; however, the performance of the mutants did not improve over time, indicating a deficit in motor learning. Poor rotarod performance suggests dysfunction of the cerebellum, since this brain region plays a crucial role in movement, motor coordination, and motor learning (Reeber et al., 2013). Studies in both rat and human have identified *SCN3A* expression in the granule, molecular, and deep cerebellar layers of the cerebellum, suggesting that *SCN3A* is expressed in excitatory granule cells as well as inhibitory cell types in the molecular layer. (Furuyama et al., 1993; Lindia and Abbadie, 2003; Whitaker et al., 2000; Whitaker et al., 2001). The patient with mutation L247P was unable to sit without support or walk at two years of age, suggesting a deficit in motor function. Additionally, the patient exhibits hypotonia, or low muscle tone, which can be partially attributed to cerebellar dysfunction (Koziol and Barker, 2013). Taken together, these results suggest a role for *Scn3a* in cerebellum-regulated motor function.

5. Conclusions

We report the identification of the novel *de novo* variant *SCN3A*-L247P in a patient with childhood epilepsy. SCN3A-L247P was demonstrated to cause a defect in trafficking, which would be predicted to functionally reduce *SCN3A* activity. Consistent with the clinical observations, *Scn3a*$^{+/Hyp}$ mice display increased seizure susceptibility, hypoactivity, and impaired motor learning. These observations support a role for *SCN3A* loss of function mutations, whether by reduced protein expression or defective trafficking, in epileptogenesis.

Supplementary Material

Refer to Web version on PubMed Central for supplementary material.

Acknowledgments

This work was supported by NIH grants to J.A.K. (NS053792) and A.E. (NS072221 and NS090319). The authors would like to thank the NHLBI GO Exome Sequencing Project and its ongoing studies which produced and provided exome variant calls for comparison: the Lung GO Sequencing Project (HL-102923), the WHI Sequencing Project (HL-102924), the Broad GO Sequencing Project (HL-102925), the Seattle GO Sequencing Project (HL-102926) and the Heart GO Sequencing Project (HL-103010). The authors would like to thank the Exome Aggregation Consortium and the groups that provided exome variant data for comparison. A full list of contributing groups can be found at http://exac.broadinstitute.org/about. We thank the patient and her family for their cooperation. We also thank the Emory Rodent Behavioral core for performing the locomotor activity task. Imaging work was performed at the Northwestern University Center for Advanced Microscopy generously supported by

CCSG P30 CA060553 awarded to the Robert H. Lurie Comprehensive Cancer Center. Imaging was performed with a CRI Nuance spectral camera purchased with support from the Avon Foundation to Charles Clevenger.

References

Baasch AL, Huning I, Gilissen C, Klepper J, Veltman JA, Gillessen-Kaesbach G, Hoischen A, Lohmann K. Exome sequencing identifies a de novo SCN2A mutation in a patient with intractable seizures, severe intellectual disability, optic atrophy, muscular hypotonia, and brain abnormalities. Epilepsia. 2014; 55:e25–9. [PubMed: 24579881]

Barton ME, Klein BD, Wolf HH, White HS. Pharmacological characterization of the 6 Hz psychomotor seizure model of partial epilepsy. Epilepsy Res. 2001; 47:217–27. [PubMed: 11738929]

Bechi G, Rusconi R, Cestele S, Striano P, Franceschetti S, Mantegazza M. Rescuable folding defective NaV1.1 (SCN1A) mutants in epilepsy: Properties, occurrence, and novel rescuing strategy with peptides targeted to the endoplasmic reticulum. Neurobiol Dis. 2015; 75:100–14. [PubMed: 25576396]

Beckh S, Noda M, Lubbert H, Numa S. Differential regulation of three sodium channel messenger RNAs in the rat central nervous system during development. EMBO J. 1989; 8:3611–6. [PubMed: 2555170]

Black JA, Yokoyama S, Higashida H, Ransom BR, Waxman SG. Sodium channel mRNAs I, II and III in the CNS: cell-specific expression. Brain Res Mol Brain Res. 1994; 22:275–89. [PubMed: 8015385]

Brown WC, Schiffman DO, Swinyard EA, Goodman LS. Comparative assay of an antiepileptic drugs by psychomotor seizure test and minimal electroshock threshold test. J Pharmacol Exp Ther. 1953; 107:273–83. [PubMed: 13035666]

Cestele S, Schiavon E, Rusconi R, Franceschetti S, Mantegazza M. Nonfunctional NaV1.1 familial hemiplegic migraine mutant transformed into gain of function by partial rescue of folding defects. Proc Natl Acad Sci U S A. 2013; 110:17546–51. [PubMed: 24101488]

Cheah CS, Westenbroek RE, Roden WH, Kalume F, Oakley JC, Jansen LA, Catterall WA. Correlations in timing of sodium channel expression, epilepsy, and sudden death in Dravet syndrome. Channels (Austin). 2013; 7:468–72. [PubMed: 23965409]

Chen C, Westenbroek RE, Xu X, Edwards CA, Sorenson DR, Chen Y, McEwen DP, O'Malley HA, Bharucha V, Meadows LS, Knudsen GA, Vilaythong A, Noebels JL, Saunders TL, Scheuer T, Shrager P, Catterall WA, Isom LL. Mice lacking sodium channel beta1 subunits display defects in neuronal excitability, sodium channel expression, and nodal architecture. J Neurosci. 2004; 24:4030–42. [PubMed: 15102918]

Chen, Y., Liao, W., Zeng, Y., Tang, B., Shi, Y., Meng, H., Xu, H., Min, F., Yu, L., Yi, Y., Li, B., Guo, J. Novel *SCN3A* mutations in epilepsy patients with febrile seizures and mental retardation. Paper presented at the 10th Asian & Oceanian Epilepsy Congress; Singapore. 2014. Abstract retrieved from http://www.epilepsysingapore2014.org/_fileupload/10th%20AOEC%20-%20Abstract%20Book.pdf

Chen YH, Dale TJ, Romanos MA, Whitaker WR, Xie XM, Clare JJ. Cloning, distribution and functional analysis of the type III sodium channel from human brain. Eur J Neurosci. 2000; 12:4281–9. [PubMed: 11122339]

Chen YJ, Shi YW, Xu HQ, Chen ML, Gao MM, Sun WW, Tang B, Zeng Y, Liao WP. Electrophysiological Differences between the Same Pore Region Mutation in SCN1A and SCN3A. Mol Neurobiol. 2015; 51:1263–70. [PubMed: 24990319]

de Kovel CG, Meisler MH, Brilstra EH, van Berkestijn FM, van 't Slot R, van Lieshout S, Nijman IJ, O'Brien JE, Hammer MF, Estacion M, Waxman SG, Dib-Hajj SD, Koeleman BP. Characterization of a de novo SCN8A mutation in a patient with epileptic encephalopathy. Epilepsy Res. 2014; 108:1511–8. [PubMed: 25239001]

Dutton SB, Makinson CD, Papale LA, Shankar A, Balakrishnan B, Nakazawa K, Escayg A. Preferential inactivation of Scn1a in parvalbumin interneurons increases seizure susceptibility. Neurobiol Dis. 2013; 49:211–20. [PubMed: 22926190]

Escayg A, Goldin AL. Sodium channel SCN1A and epilepsy: mutations and mechanisms. Epilepsia. 2010; 51:1650–8. [PubMed: 20831750]

Escayg A, MacDonald BT, Meisler MH, Baulac S, Huberfeld G, An-Gourfinkel I, Brice A, LeGuern E, Moulard B, Chaigne D, Buresi C, Malafosse A. Mutations of SCN1A, encoding a neuronal sodium channel, in two families with GEFS+2. Nat Genet. 2000; 24:343–5. [PubMed: 10742094]

Estacion M, Gasser A, Dib-Hajj SD, Waxman SG. A sodium channel mutation linked to epilepsy increases ramp and persistent current of Nav1.3 and induces hyperexcitability in hippocampal neurons. Exp Neurol. 2010; 224:362–8. [PubMed: 20420834]

Estacion M, O'Brien JE, Conravey A, Hammer MF, Waxman SG, Dib-Hajj SD, Meisler MH. A novel de novo mutation of SCN8A (Nav1.6) with enhanced channel activation in a child with epileptic encephalopathy. Neurobiol Dis. 2014; 69:117–23. [PubMed: 24874546]

Felts PA, Yokoyama S, Dib-Hajj S, Black JA, Waxman SG. Sodium channel alpha-subunit mRNAs I, II, III, NaG, Na6 and hNE (PN1): different expression patterns in developing rat nervous system. Brain Res Mol Brain Res. 1997; 45:71–82. [PubMed: 9105672]

Fung LW, Kwok SL, Tsui KW. SCN8A mutations in Chinese children with early onset epilepsy and intellectual disability. Epilepsia. 2015; 56:1319–20. [PubMed: 26235738]

Furuyama T, Morita Y, Inagaki S, Takagi H. Distribution of I, II and III subtypes of voltage-sensitive Na+ channel mRNA in the rat brain. Brain Res Mol Brain Res. 1993; 17:169–73. [PubMed: 8381901]

Hackenberg A, Baumer A, Sticht H, Schmitt B, Kroell-Seger J, Wille D, Joset P, Papuc S, Rauch A, Plecko B. Infantile epileptic encephalopathy, transient choreoathetotic movements, and hypersomnia due to a De Novo missense mutation in the SCN2A gene. Neuropediatrics. 2014; 45:261–4. [PubMed: 24710820]

Hamill OP, Marty A, Neher E, Sakmann B, Sigworth FJ. Improved patch-clamp techniques for high-resolution current recording from cells and cell-free membrane patches. Pflugers Arch. 1981; 391:85–100. [PubMed: 6270629]

Han S, Tai C, Westenbroek RE, Yu FH, Cheah CS, Potter GB, Rubenstein JL, Scheuer T, de la Iglesia HO, Catterall WA. Autistic-like behaviour in Scn1a+/− mice and rescue by enhanced GABA-mediated neurotransmission. Nature. 2012; 489:385–90. [PubMed: 22914087]

Heron SE, Crossland KM, Andermann E, Phillips HA, Hall AJ, Bleasel A, Shevell M, Mercho S, Seni MH, Guiot MC, Mulley JC, Berkovic SF, Scheffer IE. Sodium-channel defects in benign familial neonatal-infantile seizures. Lancet. 2002; 360:851–2. [PubMed: 12243921]

Holland KD, Kearney JA, Glauser TA, Buck G, Keddache M, Blankston JR, Glaaser IW, Kass RS, Meisler MH. Mutation of sodium channel SCN3A in a patient with cryptogenic pediatric partial epilepsy. Neurosci Lett. 2008; 433:65–70. [PubMed: 18242854]

Howell KB, McMahon JM, Carvill GL, Tambunan D, Mackay MT, Rodriguez-Casero V, Webster R, Clark D, Freeman JL, Calvert S, Olson HE, Mandelstam S, Poduri A, Mefford HC, Harvey AS, Scheffer IE. SCN2A encephalopathy: A major cause of epilepsy of infancy with migrating focal seizures. Neurology. 2015; 85:958–66. [PubMed: 26291284]

Koziol LF, Barker LA. Hypotonia, jaundice, and Chiari malformations: relationships to executive functions. Appl Neuropsychol Child. 2013; 2:141–9. [PubMed: 23848246]

Lindia JA, Abbadie C. Distribution of the voltage gated sodium channel Na(v)1.3-like immunoreactivity in the adult rat central nervous system. Brain Res. 2003; 960:132–41. [PubMed: 12505665]

Lossin C, Wang DW, Rhodes TH, Vanoye CG, George AL Jr. Molecular basis of an inherited epilepsy. Neuron. 2002; 34:877–84. [PubMed: 12086636]

Maier T, Guell M, Serrano L. Correlation of mRNA and protein in complex biological samples. FEBS Lett. 2009; 583:3966–73. [PubMed: 19850042]

Makinson CD, Tanaka BS, Lamar T, Goldin AL, Escayg A. Role of the hippocampus in Nav1.6 (Scn8a) mediated seizure resistance. Neurobiol Dis. 2014; 68:16–25. [PubMed: 24704313]

Martin MS, Tang B, Papale LA, Yu FH, Catterall WA, Escayg A. The voltage-gated sodium channel Scn8a is a genetic modifier of severe myoclonic epilepsy of infancy. Hum Mol Genet. 2007; 16:2892–9. [PubMed: 17881658]

Nie L, Wu G, Zhang W. Correlation of mRNA expression and protein abundance affected by multiple sequence features related to translational efficiency in Desulfovibrio vulgaris: a quantitative analysis. Genetics. 2006; 174:2229–43. [PubMed: 17028312]

Papale LA, Makinson CD, Christopher Ehlen J, Tufik S, Decker MJ, Paul KN, Escayg A. Altered sleep regulation in a mouse model of SCN1A-derived genetic epilepsy with febrile seizures plus (GEFS +). Epilepsia. 2013; 54:625–34. [PubMed: 23311867]

Petrovski S, Wang Q, Heinzen EL, Allen AS, Goldstein DB. Genic intolerance to functional variation and the interpretation of personal genomes. PLoS Genet. 2013; 9:e1003709. [PubMed: 23990802]

Pfaffl MW. A new mathematical model for relative quantification in real-time RT-PCR. Nucleic Acids Res. 2001; 29:e45. [PubMed: 11328886]

Racine RJ. Modification of seizure activity by electrical stimulation. II. Motor seizure. Electroencephalogr Clin Neurophysiol. 1972; 32:281–94. [PubMed: 4110397]

Raj A, Peskin CS, Tranchina D, Vargas DY, Tyagi S. Stochastic mRNA synthesis in mammalian cells. PLoS Biol. 2006; 4:e309. [PubMed: 17048983]

Ramos RL, Smith PT, DeCola C, Tam D, Corzo O, Brumberg JC. Cytoarchitecture and transcriptional profiles of neocortical malformations in inbred mice. Cereb Cortex. 2008; 18:2614–28. [PubMed: 18308707]

Reeber SL, Otis TS, Sillitoe RV. New roles for the cerebellum in health and disease. Front Syst Neurosci. 2013; 7:83. [PubMed: 24294192]

Rusconi R, Combi R, Cestele S, Grioni D, Franceschetti S, Dalpra L, Mantegazza M. A rescuable folding defective Nav1.1 (SCN1A) sodium channel mutant causes GEFS+: common mechanism in Nav1.1 related epilepsies? Hum Mutat. 2009; 30:E747–60. [PubMed: 19402159]

Rusconi R, Scalmani P, Cassulini RR, Giunti G, Gambardella A, Franceschetti S, Annesi G, Wanke E, Mantegazza M. Modulatory proteins can rescue a trafficking defective epileptogenic Nav1.1 Na+ channel mutant. J Neurosci. 2007; 27:11037–46. [PubMed: 17928445]

Sawyer NT, Papale LA, Eliason J, Neigh GN, Escayg A. Scn8a voltage-gated sodium channel mutation alters seizure and anxiety responses to acute stress. Psychoneuroendocrinology. 2014; 39:225–36. [PubMed: 24138934]

Scheffer IE, Zhang YH, Jansen FE, Dibbens L. Dravet syndrome or genetic (generalized) epilepsy with febrile seizures plus? Brain Dev. 2009; 31:394–400. [PubMed: 19203856]

Schwarz N, Hahn A, Bast T, Muller S, Loffler H, Maljevic S, Gaily E, Prehl I, Biskup S, Joensuu T, Lehesjoki AE, Neubauer BA, Lerche H, Hedrich UB. Mutations in the sodium channel gene SCN2A cause neonatal epilepsy with late-onset episodic ataxia. J Neurol. 2016; 263:334–43. [PubMed: 26645390]

Sievers F, Wilm A, Dineen D, Gibson TJ, Karplus K, Li W, Lopez R, McWilliam H, Remmert M, Soding J, Thompson JD, Higgins DG. Fast, scalable generation of high-quality protein multiple sequence alignments using Clustal Omega. Mol Syst Biol. 2011; 7:539. [PubMed: 21988835]

Sugawara T, Tsurubuchi Y, Agarwala KL, Ito M, Fukuma G, Mazaki-Miyazaki E, Nagafuji H, Noda M, Imoto K, Wada K, Mitsudome A, Kaneko S, Montal M, Nagata K, Hirose S, Yamakawa K. A missense mutation of the Na+ channel alpha II subunit gene Na(v)1.2 in a patient with febrile and afebrile seizures causes channel dysfunction. Proc Natl Acad Sci U S A. 2001; 98:6384–9. [PubMed: 11371648]

Surovy M, Soltysova A, Kolnikova M, Sykora P, Ilencikova D, Ficek A, Radvanszky J, Kadasi L. Novel SCN1A variants in Dravet syndrome and evaluating a wide approach of patient selection. Gen Physiol Biophys. 2016

Tang B, Dutt K, Papale L, Rusconi R, Shankar A, Hunter J, Tufik S, Yu FH, Catterall WA, Mantegazza M, Goldin AL, Escayg A. A BAC transgenic mouse model reveals neuron subtype-specific effects of a Generalized Epilepsy with Febrile Seizures Plus (GEFS+) mutation. Neurobiol Dis. 2009; 35:91–102. [PubMed: 19409490]

Thompson CH, Porter JC, Kahlig KM, Daniels MA, George AL Jr. Nontruncating SCN1A mutations associated with severe myoclonic epilepsy of infancy impair cell surface expression. J Biol Chem. 2012; 287:42001–8. [PubMed: 23086956]

Toman JE. Neuropharmacologic considerations in psychic seizures. Neurology. 1951; 1:444–60. [PubMed: 14899586]

Vaher U, Noukas M, Nikopensius T, Kals M, Annilo T, Nelis M, Ounap K, Reimand T, Talvik I, Ilves P, Piirsoo A, Seppet E, Metspalu A, Talvik T. De novo SCN8A mutation identified by whole-exome sequencing in a boy with neonatal epileptic encephalopathy, multiple congenital anomalies, and movement disorders. J Child Neurol. 2014; 29:NP202–6. [PubMed: 24352161]

Vanoye CG, Gurnett CA, Holland KD, George AL Jr, Kearney JA. Novel SCN3A variants associated with focal epilepsy in children. Neurobiol Dis. 2014; 62:313–22. [PubMed: 24157691]

Vanoye CG, Lossin C, Rhodes TH, George AL Jr. Single-channel properties of human NaV1.1 and mechanism of channel dysfunction in SCN1A-associated epilepsy. J Gen Physiol. 2006; 127:1–14. [PubMed: 16380441]

Veeramah KR, O'Brien JE, Meisler MH, Cheng X, Dib-Hajj SD, Waxman SG, Talwar D, Girirajan S, Eichler EE, Restifo LL, Erickson RP, Hammer MF. De novo pathogenic SCN8A mutation identified by whole-genome sequencing of a family quartet affected by infantile epileptic encephalopathy and SUDEP. Am J Hum Genet. 2012; 90:502–10. [PubMed: 22365152]

Volkers L, Kahlig KM, Verbeek NE, Das JH, van Kempen MJ, Stroink H, Augustijn P, van Nieuwenhuizen O, Lindhout D, George AL Jr, Koeleman BP, Rook MB. Nav 1.1 dysfunction in genetic epilepsy with febrile seizures-plus or Dravet syndrome. Eur J Neurosci. 2011; 34:1268–75. [PubMed: 21864321]

Wang DW, Mistry AM, Kahlig KM, Kearney JA, Xiang J, George AL Jr. Propranolol blocks cardiac and neuronal voltage-gated sodium channels. Front Pharmacol. 2010; 1:144. [PubMed: 21833183]

Whitaker WR, Clare JJ, Powell AJ, Chen YH, Faull RL, Emson PC. Distribution of voltage-gated sodium channel alpha-subunit and beta-subunit mRNAs in human hippocampal formation, cortex, and cerebellum. J Comp Neurol. 2000; 422:123–39. [PubMed: 10842222]

Whitaker WR, Faull RL, Waldvogel HJ, Plumpton CJ, Emson PC, Clare JJ. Comparative distribution of voltage-gated sodium channel proteins in human brain. Brain Res Mol Brain Res. 2001; 88:37–53. [PubMed: 11295230]

Yu FH, Mantegazza M, Westenbroek RE, Robbins CA, Kalume F, Burton KA, Spain WJ, McKnight GS, Scheuer T, Catterall WA. Reduced sodium current in GABAergic interneurons in a mouse model of severe myoclonic epilepsy in infancy. Nat Neurosci. 2006; 9:1142–9. [PubMed: 16921370]

Highlights

- A de novo *SCN3A* mutation, L247P, was identified in a patient with focal epilepsy.
- *SCN3A* L247P mutation reduces cell surface expression of *SCN3A*.
- A hypomorphic *Scn3a* allele (*Scn3a*$^{+/Hyp}$) increases seizure susceptibility in mice.
- *Scn3a*$^{+/Hyp}$ mutants exhibit impaired motor behavior and motor learning.

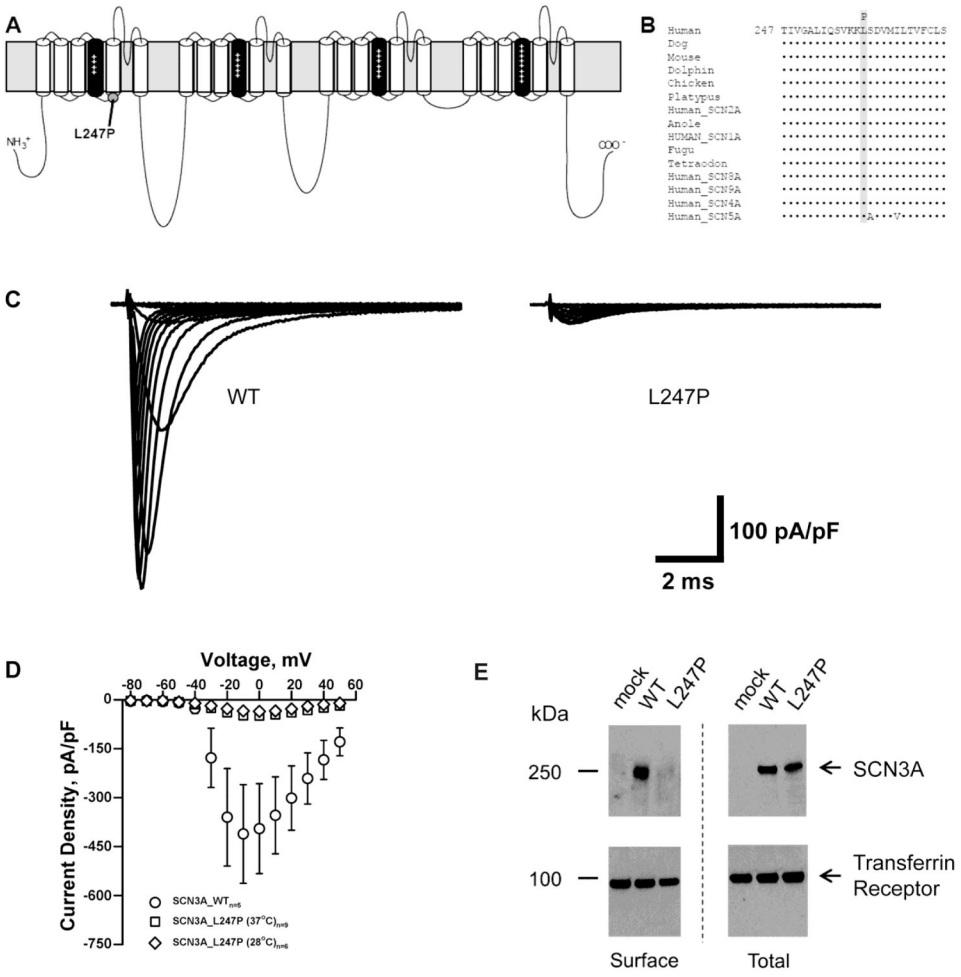

Fig. 1.

SCN3A-L247P is a trafficking deficient mutant. (A) Predicted transmembrane topology of $Na_V1.3$ showing the location of the L247P variant characterized in this study. The S4 segments are shown in black with plus (+) signs and the grey rectangle behind the depiction represents the plasma membrane. (B) Multiple alignment of human homologs and species orthologs of $Na_V1.3$ (Clustal Omega; (Sievers et al., 2011)). The variant amino acid L247P (shaded) is contained within a region of strong evolutionary conservation. (C) Average sodium current traces for SCN3A-WT and SCN3A-L247P co-expressed with β1 and β2 in a heterologous expression system (tsA201 cells). (D) Average current density-voltage relationships are shown for whole-cell currents tsA201 cells transiently co-expressing β1 and β2 with SCN3A-WT or SCN3A-L247P incubated at 37°C or 28°C for 24 hours prior to recording. (E) Total and surface protein were detected with anti-pan VGSC α subunit antibody or anti-transferrin receptor antibody as indicated. The WT SCN3A protein traffics normally to the cell surface, whereas trafficking of SCN3A L247P to the cell surface is significantly impaired.

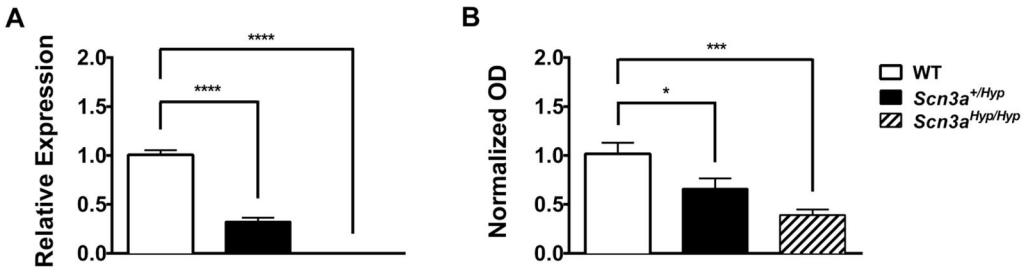

Fig. 2.

Scn3a expression is reduced in $Scn3a^{+/Hyp}$ mice. (A) *Scn3a* mRNA expression is reduced by approximately 70% ($p < 0.0001$) and nearly 100% ($p < 0.0001$) in $Scn3a^{+/Hyp}$ and $Scn3a^{Hyp/Hyp}$ mice respectively. mRNA expression, quantified from real-time PCR analysis, was normalized to β-actin. Expression values for each genotype are relative to WT levels. n = 4 (WT), 5 ($Scn3a^{+/Hyp}$), 3 ($Scn3a^{Hyp/Hyp}$). (B) Scn3a protein expression, quantified from Western blot analysis, is reduced by approximately 35% ($p < 0.05$) and 60% ($p < 0.001$) in membrane-enriched whole brain homogenate from $Scn3a^{+/Hyp}$ and $Scn3a^{Hyp/Hyp}$ mice, respectively. Optical density (OD) expression values are relative to WT and normalized to α-tubulin; n = 5 (WT), 6 ($Scn3a^{+/Hyp}$), 4 ($Scn3a^{Hyp/Hyp}$). Protein results represent the means of triplicate values for each genotype. *$p < 0.05$, *** < 0.001, ****$p < 0.0001$; One-way ANOVA. Error bars indicate SEM.

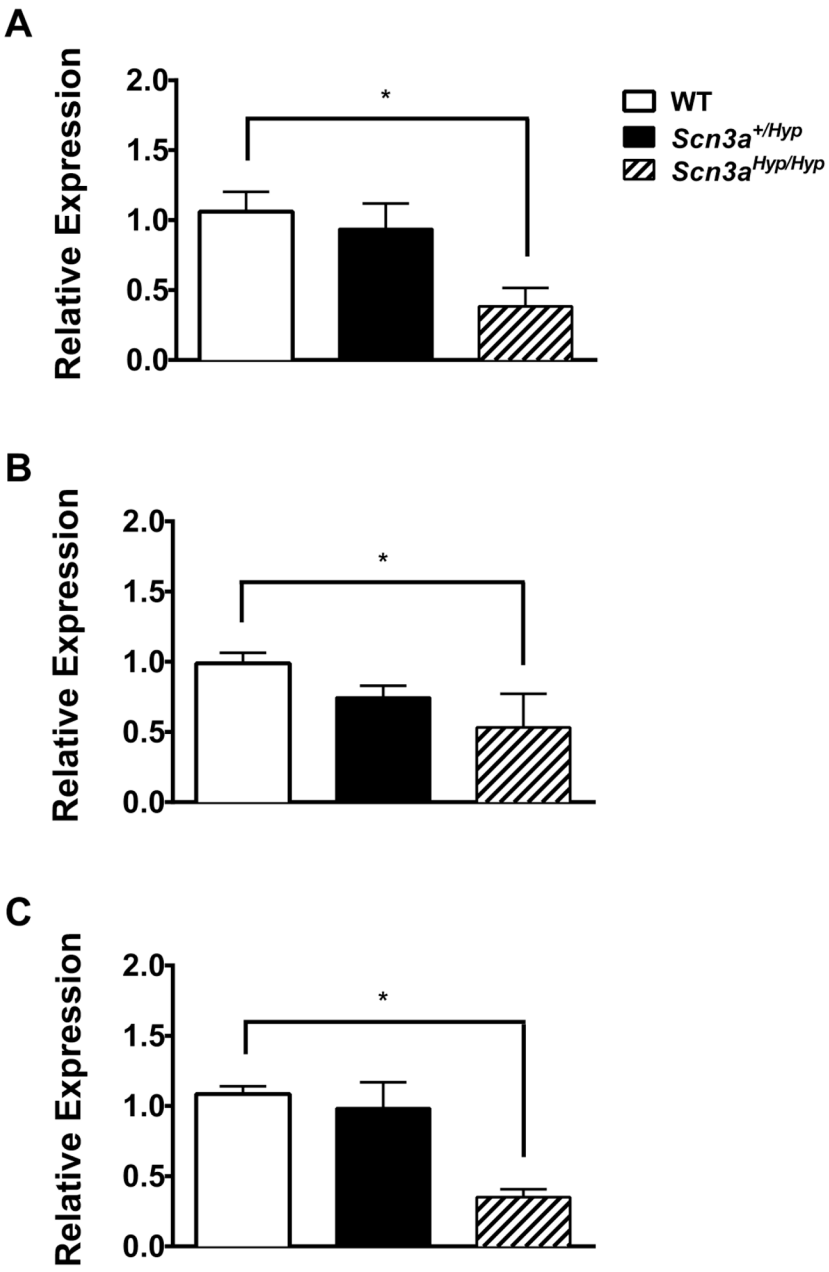

Fig. 3.

Expression of *Scn1a*, *Scn2a*, and *Scn8a* in *Scn3a*$^{+/Hyp}$ mice. (A) *Scn1a*, (B) *Scn2a*), and (C) *Scn8a* mRNA expression, quantified from real-time PCR analysis, is significantly reduced in whole brain samples from P1 *Scn3a*$^{Hyp/Hyp}$ mice. n = 4 (WT), 5 (*Scn3a*$^{+/Hyp}$), 3 (*Scn3a*$^{Hyp/Hyp}$). Expression values are relative to WT and normalized to β-actin. *$p < 0.05$, One-way ANOVA. Error bars indicate SEM.

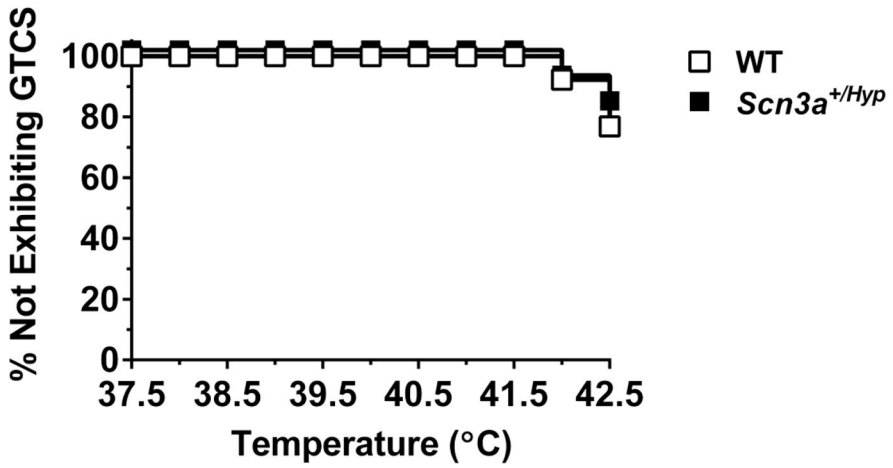

Fig. 4.

Scn3a$^{+/Hyp}$ mice do not exhibit increased susceptibility to hyperthermia-induced seizures. Seizure generation in response to increasing body temperature was comparable between *Scn3a*$^{+/Hyp}$ mutants (n = 12) and WT littermates (n = 13). Log-Rank Survival Test.

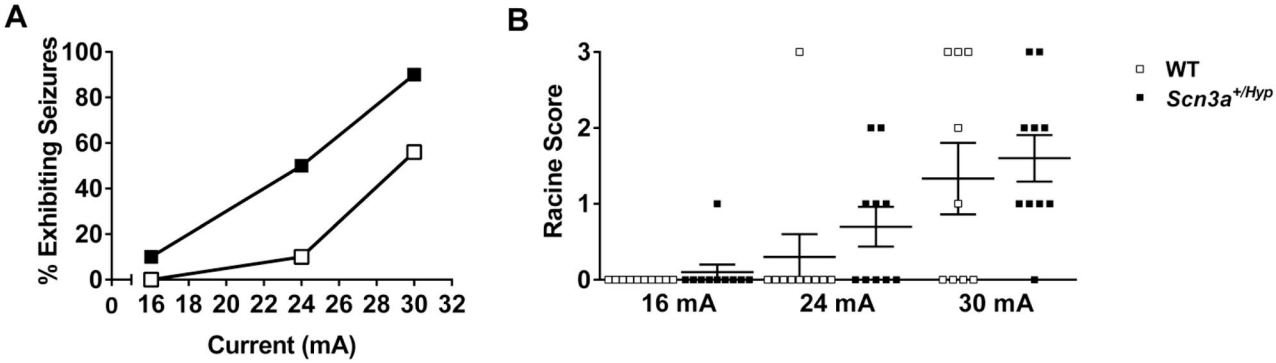

Fig. 5.

Scn3a$^{+/Hyp}$ mice exhibit increased susceptibility to 6 Hz psychomotor seizures. (A) The CC_{50} is significantly lower for *Scn3a*$^{+/Hyp}$ mice compared with WT littermates; n = 10/genotype. (B) The difference in the average Racine score between *Scn3a*$^{+/Hyp}$ mutants and WT littermates was not statistically significant for any current. Mann-Whitney Rank Sum test. Error bars indicate SEM.

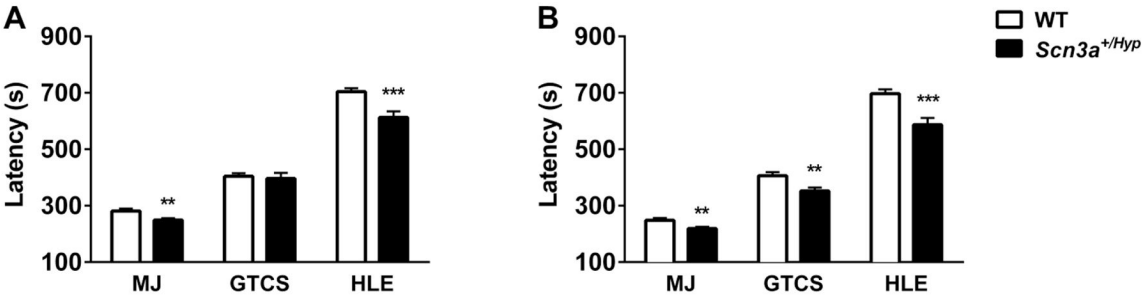

Fig. 6.

Scn3a$^{+/Hyp}$ mice exhibit increased susceptibility to flurothyl-induced seizures. (A) Male *Scn3a*$^{+/Hyp}$ mutants exhibit significantly shorter latencies to the first MJ and HLE when compared to WT littermates. (B) Female *Scn3a*$^{+/Hyp}$ female mice have significantly shorter latencies to all three seizure components when compared to WT; male n = 33 (WT), 29 (*Scn3a*$^{+/Hyp}$); female n = 32 (WT), 29 (*Scn3a*$^{+/Hyp}$). **p < 0.01, ***p < 0.001, Two-tailed Student's t-test. Error bars indicate SEM.

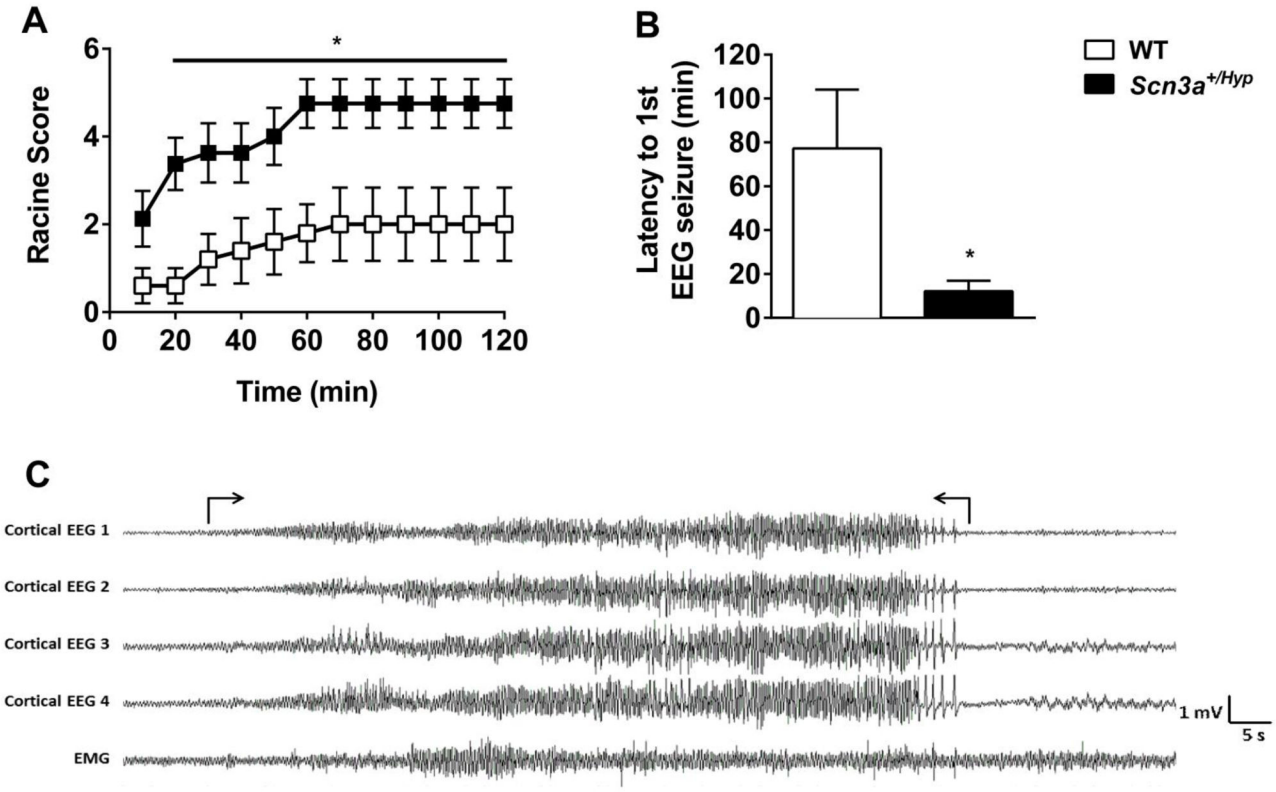

Fig. 7.

Scn3a$^{+/Hyp}$ mice exhibit increased susceptibility to KA-induced seizures. (A) Following the administration of KA, *Scn3a*$^{+/Hyp}$ mutants (n = 8) exhibited significantly more severe seizure phenotypes when compared to WT littermates (n = 5). *p < 0.05; Two-way repeated measures ANOVA. (B) Average latency to the first electrographic seizure was shorter in *Scn3a*$^{+/Hyp}$ mutants. *p < 0.05, Two-tailed Student's t-test. (C) A representative EEG recording during a KA-induced seizure in a mutant mouse. Seizure onset and termination are indicated within brackets. EEG montage: Cortical EEG 1, Cortical EEG 2, Cortical EEG 3, and Cortical EEG 4 – cortical electrodes. EMG – muscle electrodes. All cortical electrodes and EMG referenced to a second EMG electrode. Error bars indicate SEM.

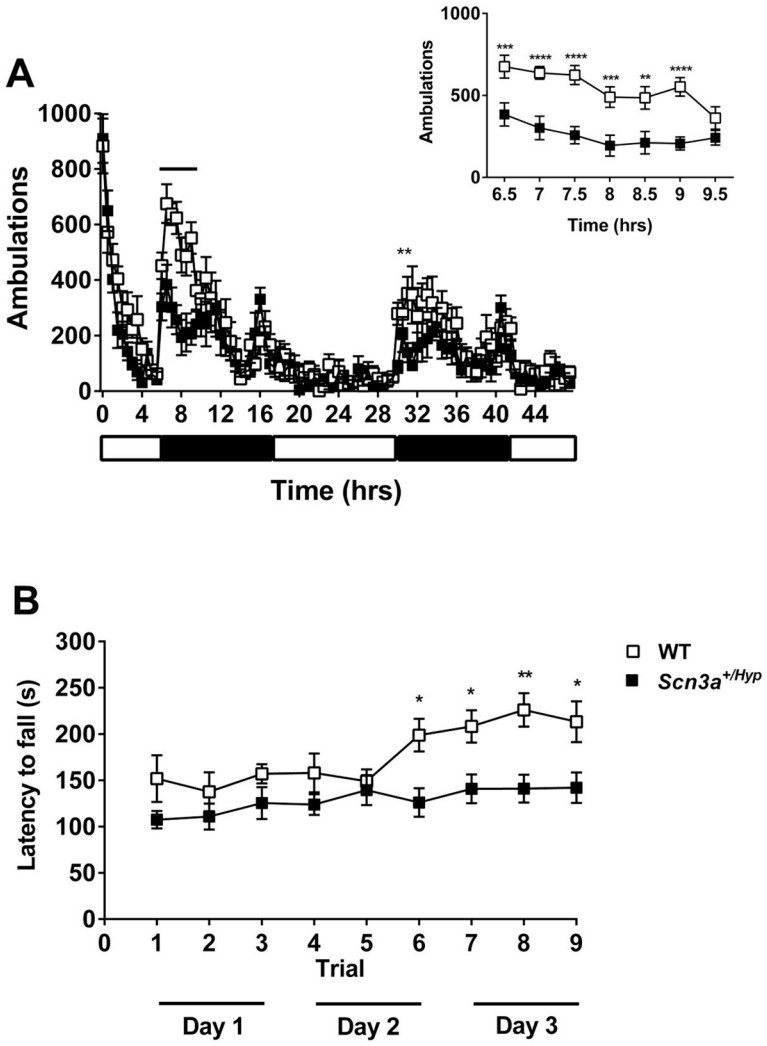

Fig. 8.

Scn3a$^{+/Hyp}$ mice exhibit deficits in motor behavior. (A) *Scn3a*$^{+/Hyp}$ mice (n = 8) traveled significantly less than WT (n = 8) during the first dark phase (hours 6.5–9.5) and the second dark phase (hour 31.5–32.0). Inset shows locomotor activity during hours 6.5–9.5. **p < 0.01, ***p < 0.001, ****p < 0.0001; Two-way repeated measures ANOVA (Genotype × Time). White and black bars below the X-axis represent the light and dark periods, respectively. (B) Latency to fall from the rotarod was significantly shorter for *Scn3a*$^{+/Hyp}$ mutants (n = 11) when compared to WT littermates (n = 9) from trial 6 (Day 2) to the last trial (trial 9) on Day 3. *p < 0.05, **p < 0.01, Two-way repeated measures ANOVA (Genotype × Time). Error bars indicate SEM.